Environmental Technology & Innovation 41 (2026) 104686

Contents lists available at ScienceDirect

Environmental Technology & Innovation

journal homepage: www.elsevier.com/locate/eti

Integration of struvite precipitation and membrane stripping in a single reactor for dual nutrient recovery: A feasibility assessment with synthetic wastewater

Bogna Śniatała [a], Dominika Sobotka [a], Marta Ippolito [b], Francesco Giannici [b], Giorgio Mannina [c], Jacek Mąkinia [a,*]

[a] Faculty of Civil and Environmental Engineering, Gdansk University of Technology, Narutowicza 11/12, Gdansk 80-233, Poland
[b] Department of Physics and Chemistry, University of Palermo, Viale delle Scienze, Palermo 90128, Italy
[c] Department of Engineering, University of Palermo, Viale delle Scienze, Palermo 90128, Italy

ARTICLE INFO

Keywords:
Chemical precipitation
Gas-permeable membrane
Integrated nutrient recovery
Membrane stripping
Process optimization

ABSTRACT

Integrating complementary nitrogen (N)- and phosphorus (P)-oriented recovery processes is crucial for advancing wastewater treatment plants toward water resource recovery facilities. This study proposes an innovative one-reactor system for dual nutrient recovery, combining P chemical precipitation and ammonia (NH_3) absorption into acid via gas-to-liquid membrane stripping (GLMS), using elevated temperature (T) and alkaline pH to promote both struvite formation and NH_3 volatilization. Laboratory-scale batch tests were performed using synthetic wastewater to evaluate the integrated technology feasibility and understand the effects of pH (7.3–10.0), T (20–50°C), and feed concentration (1.0–3.0 $gNdm^{-3}$; 0.4–1.2 $gPdm^{-3}$) on recovery performance and product purity. The system achieved up to 99.3 %P and 93.1 %N recovery, with GLMS increasing N recovery by 37.0 ± 24.6 % compared to struvite precipitation alone, though the dominant N recovery pathway (crystallization vs. absorption) depended on the applied operational conditions. Struvite was the dominant P phase at pH ≤ 9.0, whereas highly alkaline and thermal conditions, together with a higher feed concentration, affected product purity and homogeneity. Conversely, elevated pH and T were the main drivers of NH_3 volatilization, showcasing the mutual effect of NH_3 stripping and struvite precipitation. Operation under moderate conditions (pH 8.0–9.0, 38–41°C) yielded high-purity struvite (~100.0 %), > 93.0 %P and > 40.0 %N recovery effectiveness. This study demonstrates the feasibility of integrating struvite precipitation with NH_3-oriented GLMS in a compact system for enhanced nutrient recovery from wastewater, enabling the production of two wastewater-derived fertilizers while reducing spatial footprint, energy consumption, and chemical demand compared to conventional two-stage N and P recovery systems.

1. Introduction

The transformation of wastewater treatment plants (WWTPs) into water resource recovery facilities is critical for advancing circular economy goals in the wastewater sector. A key aspect of this transition is the integration of complementary nitrogen (N)- and

* Corresponding author.
E-mail address: jmakinia@pg.edu.pl (J. Mąkinia).

https://doi.org/10.1016/j.eti.2025.104686
Received 7 October 2025; Received in revised form 3 December 2025; Accepted 7 December 2025
Available online 8 December 2025

phosphorus (P)-oriented recovery processes from wastewater streams (Aryampa et al., 2025), which can improve overall nutrient removal efficiency while enabling resource valorization (Farghali et al., 2024). In line with this sustainable approach, the new EU Urban Wastewater Directive (EU 2024/, 3019) promotes the adoption of nutrient recovery technologies in wastewater treatment practices (Renfrew et al., 2024). With the growing interest, there is a pressing need to develop compact and efficient systems capable of simultaneously recovering both N and P (Wu and Vaneeckhaute, 2022).

Existing nutrient recovery technologies can be implemented as either single- or multi-stage systems. Single-stage processes, such as struvite ($MgNH_4PO_4{\cdot}6\,H_2O$) precipitation, biological nutrient uptake, ion-exchange/adsorption, and electrochemical or bio-electrochemical separation, enable simultaneous N and P recovery, but require high chemical and energy inputs (Wu and Vaneeckhaute, 2022; Meena et al., 2019; Wan et al., 2023). Among these, struvite precipitation is the most commonly used method, achieving nearly complete P recovery. However, it captures only a small fraction (<20 %) of the available N due to the fixed N:P molar ratio in the chemical formula of struvite (Mehta et al., 2015). The remaining N is usually discharged with the effluent or lost through volatilization, especially under highly alkaline conditions.

The two-stage processes are less common and typically involve struvite precipitation followed by NH_3 air stripping (Ndeddy Aka et al., 2025), a sequence driven by the requirement of ammonium (NH_4^+) for struvite formation (Q. Liu et al., 2024). Alternatives to P precipitation include sludge dissolution in phosphoric acid, incineration of dewatered sewage sludge to produce P-rich ash, and manure pelletizing (Brandstätter et al., 2025). While two-stage systems allow for optimization of each individual process and can achieve near-complete nutrient recovery (Wu and Vaneeckhaute, 2022), they require larger spatial footprints and increased operational complexity (Śniatała et al., 2024).

Attempts to integrate struvite precipitation with conventional air stripping (Cao et al., 2019) or vacuum thermal stripping (Tian et al., 2019) within a single reactor have shown promise, post-processing is still required to produce usable NH_4^+ salts (Wu and Vaneeckhaute, 2022). To overcome this, Pradhan et al. (Pradhan et al., 2019) proposed a combined approach using chemical P crystallization and liquid-to-liquid membrane stripping (LLMS) for direct free ammonia (NH_3) absorption in sulfuric acid (H_2SO_4) circulating in the hydrophobic gas-permeable membrane (GPM). However, the direct contact of membrane with the feed solution can lead to clogging by precipitates and biofouling, which pose operational challenges, such as reduced recovery efficiency and hydrophobicity loss (Tran et al., 2025).

The high recovery effectiveness of both P crystallization and NH_3 capture can be achieved under elevated temperature ($T > 20\ ^\circ C$) and alkaline pH conditions (Melgaço et al., 2021; Pradhan et al., 2019). pH adjustment is commonly achieved using sodium hydroxide (NaOH) (Wu and Vaneeckhaute, 2022), but excess Na^+ competes with magnesium (Mg^{2+}) ions during struvite formation (Hollas et al., 2021), potentially leading to the formation of alternative struvite-like compounds and decreasing product purity (Sangeetha et al., 2022). Magnesium hydroxide ($Mg(OH)_2$), also known as brucite, provides a promising alternative, as it simultaneously increases pH and supplies Mg^{2+} ions, thereby improving precipitation efficiency, increasing the purity of the recovered product, and reducing reliance on additional chemical inputs (Guan et al., 2023).

This study proposes an innovative single-stage system that integrates P crystallization with NH_3-oriented gas-to-liquid membrane stripping (GLMS) to improve process effectiveness and stability, and simplify operation. The specific objectives of this study are to: (i) demonstrate the feasibility of integrating struvite precipitation and NH_3-oriented GLMS in a single-reactor configuration, (ii) optimize

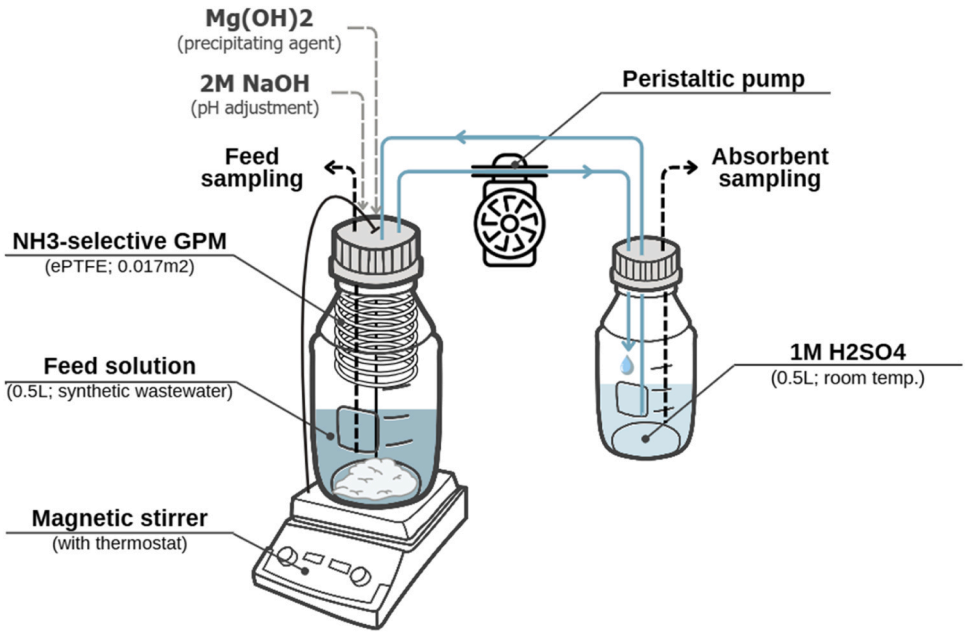

Fig. 1. Schematic diagram of the one-reactor integrated chemical precipitation and GLMS experimental unit.

operating conditions (process T and pH) to maximize recovery effectiveness while minimizing chemical and energy inputs, (iv) assess the quality of the recovered fertilizers and compare the process with other single-stage N and P recovery technologies. A series of batch tests using synthetic wastewater was conducted under laboratory conditions. The single-reactor system was operated under elevated T and alkaline pH to promote struvite precipitation and absorption of volatilized NH_3 into sulfuric acid, producing two reusable fertilizers: struvite and ammonium sulphate $(NH_4)_2SO_4$). The feasibility of this integrated approach demonstrates its potential to support the implementation of circular economy principles at WWTPs.

2. Material and methods

2.1. Experimental setup

The single-stage struvite chemical precipitation and GLMS unit consisted of an expanded polytetrafluoroethylene (ePTFE) GPM tube (Hanchen, China) (Table S1), two tightly sealed 0.5 dm^3 glass vessels (to prevent free NH_3 losses from the system), a peristaltic pump (Lead Fluid, China), and a magnetic stirrer with thermostat (Sunlab, Germany) enabling stable and precise temperature control (± 0.1°C) (Fig. 1).

Inside the first vessel (working volume of 1.0 dm^3) of the single-stage integrated struvite precipitation and GLMS unit, the GPM tube (0.017 m^2) was suspended above the feed solution (0.5 dm^3) to capture NH_3 stripped from the liquid phase. A sulfuric acid (H_2SO_4) solution (0.5 dm^3, kept at room temperature) was circulated from the second glass vessel (working volume of 1.0 dm^3) through the lumen of the GPM tube at a flow rate of 2 $dm^3\ h^{-1}$ using the peristaltic pump to enhance NH_3 absorption (Śniatała et al., 2025). The feed solution was continuously stirred at 200 rpm and its temperature was controlled using a magnetic stirrer with an

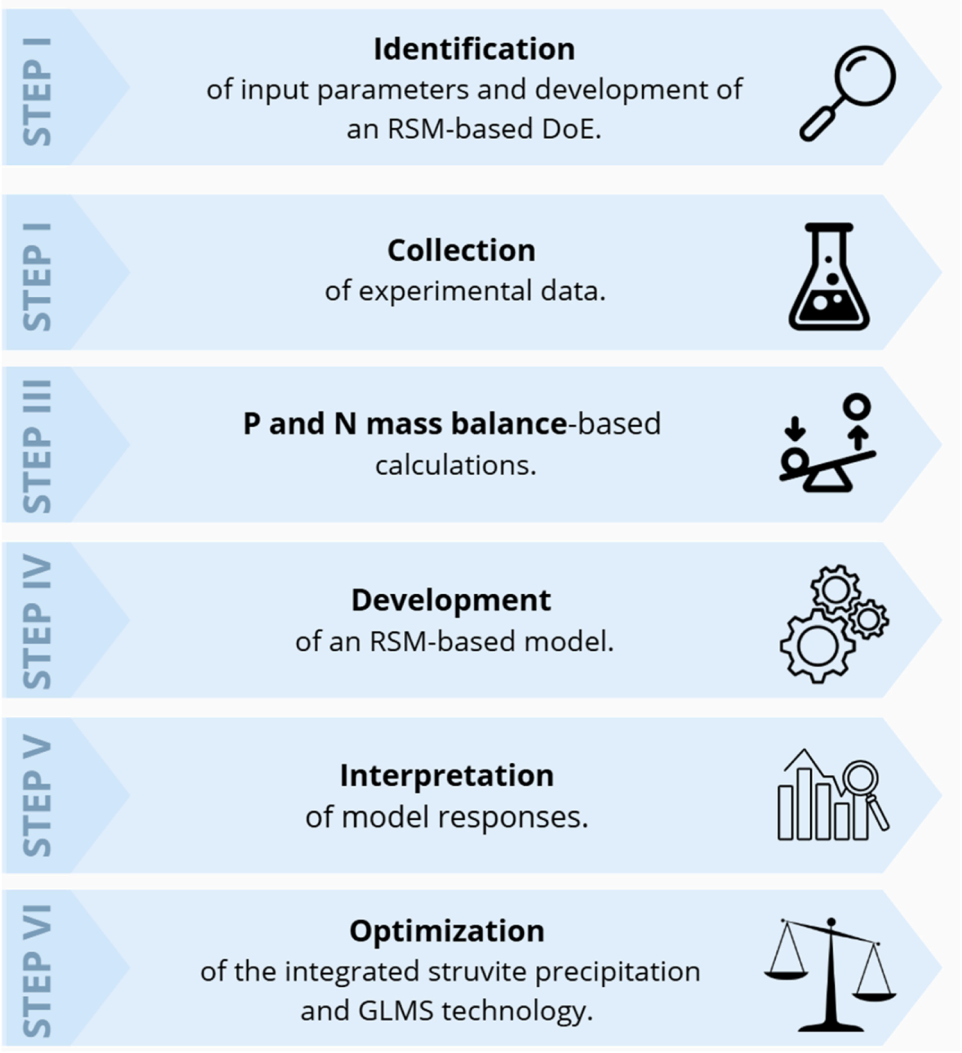

Fig. 2. Flowchart of the six-step experimental and modelling procedure.

integrated thermostat.

2.2. Design of experiments (DoE)

A systematic six-step procedure was employed to develop and optimize the innovative single-stage struvite precipitation and GLMS technology (Fig. 2). This approach included: identification of operational parameters and development of a response surface methodology (RSM)-based Design of Experiments (DoE) (step I), collection of experimental data (step II), P and N mass balance-based calculations (step III), development of RSM-based predictive models (step IV), interpretation of model responses (V), and optimization of the integrated struvite precipitation and GLMS system (step VI).

2.2.1. Identification of operational parameters and development of an RSM-based DoE

To systematically analyse the influence of key operational parameters and to identify their individual and combined effects on the performance of the novel integrated process, RSM was employed. The RSM was used to evaluate the effects of feed solution N and P concentration (C_{N_f} and C_{P_f}, respectively, with a constant N:P mass ratio of 2.5), process pH and T on several performance indicators: P and N removal and recovery effectiveness (ηP_{REM}, ηP_{REC}, ηN_{REM}, ηN_{REC}, respectively) and struvite purity ($p_{struvite}$). The Design of Experiments (DoE) was prepared using a dedicated Design Expert software (Stat-Ease, Inc., USA). A central composite design was applied, incorporating three numeric factors, influencing both struvite precipitation and GLMS (Guan et al., 2023; Serra-Toro et al., 2022; Śniatała et al., 2025): C_{N_f} 1.0–3.0 g N dm^{-3}, pH 8.0–10.0, and T (20.0–50.0°C).

To ensure the study is technically relevant and scalable, the selected parameter values were based on an in-depth literature analysis and chosen to reflect realistic conditions in WWTP side streams, particularly anaerobic digester liquors, where nutrient recovery processes are usually applied due to elevated C_{N_f} and C_{P_f} levels (Serra-Toro et al., 2022). Moreover, the tested pH and T ranges were selected to ensure both effective struvite precipitation and free NH_3 release from the feed solution (Soto-Herranz et al., 2021; Wen et al., 2021). The full factorial experimental design with two central points and an α-value of 1.68, resulted in a total number of 16 experiments (Table S2).

2.2.2. Collection of experimental data

Laboratory experiments were performed in a batch mode in accordance with the developed DoE, as described in **Section 2.3 .** Each experimental condition was tested in duplicate, with a total runtime of 21 h per test to ensure stable process performance, as indicated by preliminary trials (data not shown). For one replicate under each condition, additional precipitate analyses were performed to support N and P mass balance-based calculations and evaluate the influence of operating variables on the composition of crystallized phases. Specifically, crystallographic and fractional composition analyses were performed (Hollas et al., 2021; Sangeetha et al., 2022). The dataset from the replicate with full analytical coverage (C_{N_f} and C_{P_f} concentrations in both feed and absorbent solutions, crystallographic and fractional composition) were used for the mass balance-based calculations and RSM model development.

2.2.3. Selection of process performance indicators, mass balance-based calculations, RSM model development and interpretation

To evaluate the effects of the operational variables on process performance, including C_{N_f}, pH and T, the coefficient of determination (R^2) was calculated for each linear relationship between those variables. The analysis comprised the following key performance indicators: ηP_{REM}, ηP_{REC}, ηN_{REM}, ηN_{REC}, N absorbed via GLMS ($\eta N_{absorbed}$), N and P crystallized in struvite ($\eta N_{struvite}$, $\eta P_{struvite}$), P recovered in other crystal forms ($\eta P_{other\ forms}$), N losses (ηN_{loss}) (i.e. volatile NH_3 released from the feed solution but unabsorbed and lost to atmosphere) and struvite purity ($p_{struvite}$).

The removal efficiencies (ηP_{REM}, ηN_{REM}) and recovery effectiveness indicators (ηP_{REC}, ηN_{REC}) were determined through P and N mass balances, as described in Sections 2.5.1–2.5.2. For the key performance indicators, full quadratic polynomial RSM-based models were developed using Design Expert software. Subsequently, the full models were simplified by eliminating terms with low statistical significance (p-values > 0.2). The performance of both full and simplified models was assessed and compared based on the coefficient of determination (R^2).

To interpret the interactions between process variables (pH, T), (pH, C_{N_f}), and (T, C_{N_f}), and their effects on the selected performance indicators (ηP_{REM}, ηP_{REC}, ηN_{REM}, ηN_{REC}, $\eta N_{absorbed}$, $\eta N_{struvite}$, $\eta P_{struvite}$, $\eta P_{other\ forms}$, ηN_{loss}, $p_{struvite}$), simplified models output were visualized as contour plots generated in the Design Expert software. In each plot, two process variables were varied within their experimental ranges, while the third variable was held constant at its midpoint. These visualizations provided insights into potential synergistic or antagonistic effects between the process variables.

2.2.4. Optimization of the integrated struvite precipitation and GLMS technology

Global multi-criteria optimization was performed using the Design Expert software, assuming 95 % confidence level. The optimization was conducted under three scenarios:

- **Scenario 1:** Maximize both ηN_{REC} and ηP_{REC} within the experimental ranges of C_{N_f}, pH and T, without imposing additional constraints on the input parameters;
- **Scenario 2:** Maximize both ηN_{REC} and ηP_{REC} while minimizing chemical and energy inputs, i.e., pH and T, respectively;
- **Scenario 3:** Prioritize struvite purity (i.e. 100 % $p_{struvite}$) over maximizing both ηN_{REC} and ηP_{REC}, under minimized pH and T.

The detailed optimization settings, including target goals, lower and upper limits, and the relative importance of each variable, used in the Design Expert software for Scenarios 1–3 are summarized in Table 1.

2.3. Operating procedure

Fresh feed (0.5 dm^3 of synthetic anaerobic digester liquors) and absorbent (0.5 dm^3 of 1-molar (1 M) H_2SO_4) solutions were prepared for each run. The synthetic liquors and the 1 M H_2SO_4 solutions were prepared by diluting diammonium phosphate $(NH_4)_2HPO_4$, ammonium chloride (NH_4Cl), sodium bicarbonate ($NaHCO_3$) (Melgaço et al., 2021; Munasinghe-Arachchige et al., 2021), and 99 % H_2SO_4, respectively, in distilled water. The synthetic liquors concentration was adjusted depending on the tested C_{N_f}. $Mg(OH)_2$ was used as a magnesium (Mg^{2+}) source to initiate struvite precipitation (Guan et al., 2023). At the beginning of each experiment, the required dose of $Mg(OH)_2$ to achieve the initial Mg:P molar ratio equal 1.5 (Melgaço et al., 2021) was diluted in a small volume of distilled water and introduced to the reactor using a syringe. Despite $Mg(OH)_2$ can be applied as both struvite precipitating and pH correction agent, to simultaneously maintain targeted pH and Mg:P molar ratio, the feed solution pH was corrected further after injecting $Mg(OH)_2$ using 2-molar (2 M) sodium hydroxide (NaOH) (Wu and Vaneeckhaute, 2022). The pH was adjusted with continuous monitoring by WTW™ SenTix probe.

To evaluate the process performance, total ammonia nitrogen (TAN) and phosphate phosphorus (PO_4^{3-}-P) load in both the feed and absorbent solutions were analyzed at the start and end of each run. Immediately after the process was completed, prior to analysis, the feed solution was filtered using a pre-dried and pre-weighed qualitative filter paper (MN 615) to separate the crystallized product. The collected precipitate was subsequently dried in a desiccator at room temperature for 7 days (Zaffar et al., 2024), and weighed to determine the quantity of the crystallized material. After each test, the experimental unit was cleaned and rinsed with deionized water to prevent contamination.

Table 1
Process optimization assumptions for Scenarios 1-3.

	Optimization objectives	Input/Output parameters		Target goal	Lower limit	Upper limit	Relative importance*
Scenario 1	**Maximize ηN_{REC} and ηP_{REC}**	**Input**	**pH [-]**	In range	8	10	-
			T [°C]		20	50	
			C_{N_f} [g N dm^{-3}]		1	3	
		Output	**ηP_{REC} [%]**	Target 100 %	0	100	+ ++ ++
			ηN_{REC} [%]				
			ηN_{REM} [%]	None	0	100	-
			$\eta N_{absorbed}$ [%]				
			$\eta N_{struvite}$ [%]				
			$\eta P_{struvite}$ [%]				
			$p_{struvite}$ [%]				
Scenario 2	**Maximize ηN_{REC} and ηP_{REC} and minimize chemicals and energy requirements**	**Input**	**pH [-]**	Minimize	8	10	+ +
			T [°C]		20	50	
			C_{N_f} [g N dm^{-3}]	In range	1	3	-
		Output	**ηP_{REC} [%]**	Target 100 %	0	100	+ ++ ++
			ηN_{REC} [%]				
			ηN_{REM} [%]	None	0	100	-
			$\eta N_{absorbed}$ [%]				
			$\eta N_{struvite}$ [%]				
			$\eta P_{struvite}$ [%]				
			$p_{struvite}$ [%]				
Scenario 3	**Maximize ηN_{REC} and ηP_{REC} and prioritize $p_{struvite}$**	**Input**	**pH [-]**	Minimize	8	10	+ +
			T [°C]		20	50	
			C_{N_f} [g N dm^{-3}]	In range	1	3	-
		Output	**ηP_{REC} [%]**	Target 100 %	0	100	+ ++ +
			ηN_{REC} [%]				
			ηN_{REM} [%]	None	0	100	-
			$\eta N_{absorbed}$ [%]				
			$\eta N_{struvite}$ [%]				
			$\eta P_{struvite}$ [%]				
			$p_{struvite}$ [%]	Target 100 %	0	100	+ ++ ++

* where '+ ' – very low; '+ ++ ++ ' – very high importance; '-' – not considered

2.4. Analytical methods

The TAN and PO_4^{3-}-P concentrations in the feed and absorbent solutions were measured using a colorimetric technique with ready-to-use cuvette tests (LCK Hach), following TNT834 method. For accurate analysis of samples with pH values outside the range acceptable by the method (pH 4.0–9.0), samples were neutralized with either 5-molar (5 M) NaOH or 5 M H_2SO_4 solutions. To estimate the actual N and P loads, necessary for mass balance-based calculations of the feed and absorbent solutions, their volumes were measured at the start and end of each run.

The crystallographic composition of the precipitates was analyzed by X-ray diffraction (XRD) using the MiniFlex600 diffractometer (Rigaku, Japan). Diffraction patterns were collected in Bragg-Brentano geometry with Cu K_α radiation. Phase identification was performed using the PDF-4 database (Gates-Rector and Blanton, 2019), focusing on compounds containing N, P, Mg^{2+}, oxygen (O^{2+}), and hydrogen (H^+). This targeted approach reflects the elemental composition of the synthetic feed solution and ensures selective detection of struvite and other Mg–N–P–O–H phosphate phases potentially formed under the investigated conditions (Tansel et al., 2018). The relative struvite content in the crystallized product was quantified through Rietveld refinement with the open-source crystallographic software package GSAS-II (Toby and Von Dreele, 2013). The refinement parameters included phase fractions, lattice parameters, sample displacement, crystallite size, background. In some cases, the preferential orientation of crystallites was also refined to account for non-ideal peak intensity ratios. The method provided high precision, with estimated uncertainties for all phase fractions typically ranging between 0.2–0.5 %, supporting accurate classification of the recovered products as potential fertilizers (Meira et al., 2020).

Additionally, P content in the crystallized samples (prepared as pressed powder) was determined by X-ray fluorescence (XRF) method using an XRF S1 Titan 800 analyzer (Bruker, USA), employing the GeoExploration Oxide 3 Phase protocol (Meira et al., 2020).

2.5. Data processing and calculations

2.5.1. P mass balance

In the proposed single-stage integrated system, P was removed and recovered exclusively via chemical precipitation, as P compounds are non-volatile. Accordingly, ηP_{REC} equals ηP_{REM} (Fig. 3 **a,b**), calculated as the difference in phosphorus load in the feed solution before and after the process (Eq. 1):

$$\eta PREC = \frac{\Delta[P]_f}{[P]_{f0}} \bullet 100 \quad \% \tag{1}$$

where: $\Delta[P]_f$ – change in P load difference in the feed between the start and end of the experiment [g P]; $[P]_{f0}$ – initial P load in the feed [g P]

The P load at time t is calculated as (Eq. 2):

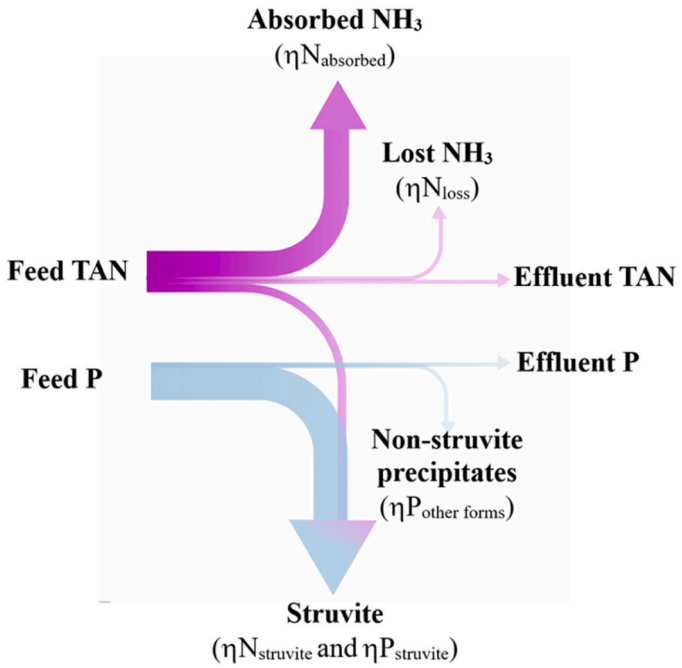

Fig. 3. Visual representation of N and P mass balances in the single-stage P precipitation and NH_3-oriented GLMS process.

$$[P]_f = C_{Pf} \bullet \quad V_f \quad [g] \tag{2}$$

where: V_f - feed volume at time t [dm^{-3}].

Furthermore, the overall P recovery (ηP_{REC}) includes P precipitated in struvite ($\eta P_{struvite}$) and other P forms ($\eta P_{other\ forms}$) (Fig. 3 **a, b**), as identified by XRD analysis (Eq. 3):

$$\eta P_{REC} = \eta P_{struvite} + \eta P_{other\ forms} \tag{3}$$

where:

$$\eta Pstruvite = \frac{m_{dw} \quad \bullet \quad p_{struvite} \quad \bullet \quad \frac{30.97}{245.41}}{[P]_{f0}} \tag{4}$$

$$\eta Pother\ forms = \sum_{i=1} \frac{m_{dw} \quad \bullet \quad p_i \quad \bullet \quad \frac{M_{P_i}}{M_i}}{[P]_{f0}} \quad [\%] \tag{5}$$

where: m_{dw} – dry weight of the precipitate [g]; $p_{struvite}$ – mass fraction of struvite [%]; p_i – mass fraction of component i in the precipitate [%]; M_{P_i} – molar mass of P in component i $\left[\frac{g\ P}{mol}\right]$; M_i – molar mass of component i $\left[\frac{g}{mol}\right]$.

An alternative estimate of P recovery, based on XRF results, is calculated as Eq. 6:

$$[P]_{prec} \quad = \quad P_{XRF} \quad \bullet m_{dw} \quad [g] \tag{6}$$

where: P_{XRF} – P content in the precipitate measured via XRF [%].

2.5.2. N mass balance

N in the feed solution exists either as free NH_3 and ionized NH_4^+ (Fig. 3 **a,b**). Free NH_3 content in the solution depends on its pH and T (Emerson et al., 1975) (Eq. 7):

$$[NH_3] = \frac{1}{1 + 10^{\left(0.0897 + \frac{2729.92}{(T+273.15)}\right) \quad -pH}} \quad \bullet 100 \quad [\%] \tag{7}$$

Due to free NH_3 volatility, N removal efficiency (ηN_{REM}) includes both N recovery (ηN_{REC}) and N loss (ηN_{loss}) (Fig. 3 **a,b**) (Eq. 8):

$$\eta N_{REM} = \eta N_{REC} + \eta N_{loss}\ [\%] \tag{8}$$

where ηN_{REM} is calculated as the difference in N load in the feed solution before and after the process (Eq. 9):

$$\eta NREM = \frac{\Delta[N]_f}{[N]_{f0}} \bullet 100 \quad \% \tag{9}$$

where: $\Delta[N]_f$ – change in N load in the feed between the start and end of the experiment [g N]; $[N]_{f0}$ – initial N load in the feed [g N] (Eq. 10):

$$[N]_f = C_{Nf} \bullet \quad V_f \quad [g] \tag{10}$$

In the integrated chemical precipitation and GLMS process, N can be recovered through both crystallization of NH_4^+ in struvite ($\eta N_{struvite}$) and absorption of free NH_3 to acidic solution via GLMS ($\eta N_{absorbed}$) (Eqs. 11–13**)**:

$$\eta N_{REC} = \eta N_{absorbed} + \eta N_{struvite}\ [\%] \tag{11}$$

$$\eta Nabsorbed = \frac{\Delta[N]_a}{[N]_{f0}} \bullet 100 \quad \% \tag{12}$$

$$\eta Nstruvite = \frac{m_{dw} \quad \bullet \quad p_{struvite} \quad \bullet \quad \frac{14.01}{245.41}}{[N]_{f0}} \quad [\%] \tag{13}$$

where: $\Delta[N]_a$ – change in N load the absorbent between the start and end of the experiment [g N] (Eq. 14); V_a – absorbent solution volume [dm^{-3}]:

$$[N]_a = C_{Na} \bullet \quad V_a \quad [g] \tag{14}$$

2.5.3. Data reconciliation

P recovery was estimated using two independent methods:

- from the P load difference in the feed, measured by LCK Hach cuvette tests ($\Delta[P]_f$); and
- from the P content in the precipitate, measured by XRF analysis ($[P]_{prec}$).

To obtain a consistent estimate of P recovery, a weighted average of the two methods was calculated using a reconciliation approach (Eq. 15):

$$[P]_{reconciled} = \frac{w_1 \bullet \Delta[P]_f + \quad w_2 \bullet [P]_{prec}}{w_1 + \quad w_2} \tag{15}$$

Weights w_1 and w_2 were determined using the Excel Solver function to minimize the total squared deviation between each method and the reconciled value (Eq. 16):

$$\text{Minimize} \sum_i \left([P]_{reconciled,i} - \overline{[P]}_i\right)^2 \tag{16}$$

where:

$$\overline{[P]}_i = \frac{\Delta[P]_{f,i} + \quad [P]_{prec,i}}{2} \tag{17}$$

Solver was constrained to find non-negative weights summing to 1.

3. Results

The conducted investigation confirmed the technical feasibility of integrating struvite precipitation and GLMS in a single-reactor system, enabling simultaneous N and P removal and recovery from synthetic anaerobic digester-like liquors. The test replicates showed good experimental repeatability, with standard deviations (SDs) not exceeding 7 % for all the measured parameters, confirming the reliability of the experimental results (Table S3).

The influence of feed composition, pH and T on the overall system performance and the characteristics of the precipitated solids was clearly observed. However, the extend of this influence varied across specific operational condition, indicating both synergistic and antagonistic interactions between the tested variables.

3.1. Impact of operational conditions on the process performance

3.1.1. Effect on the crystallized product composition

The mass of the recovered precipitate increased with nutrient concentration in the feed, ranging from 1.3 ± 0.3 g to 2.6 ± 0.7 g and 4.1 ± 0.4 g, for C_{N_f} of 1.0, 2.0 and 3.0 g N dm^{-3}, respectively (Table S4).

Crystallographic analysis detected struvite as the dominant P-containing phase, accompanied by cattiite ($Mg_3(PO_4)_2{\cdot}22\ H_2O$), bobierrite ($Mg_3(PO_4)_2{\cdot}8\ H_2O$), and brucite ($Mg(OH)_2$) (Figure S1). In addition, a significant portion of "undefined crystal phase" was found in several samples. This term refers to any phase that could not be identified using the PDF-4 database of the International Centre for Diffraction Data (ICDD).

The share of struvite ($p_{struvite}$) in the crystallized products varied widely, from 0.0 % under extreme conditions (pH 10.0, 50.0 °C, C_{N_f} = 3.0 g N dm^{-3}) to 100.0 % at pH 8.0, 50.0 °C, C_{N_f} = 1.0 g N dm^{-3}. Brucite was found in 90 % of all the tested samples, with a maximum proportion of 65.8 % at pH 9.0, 10.0°C, C_{N_f} = 2.0 g N dm^{-3}. Cattiite was present in approximately one-third of the samples, peaking at 11.6 % at pH 10.7, 35.0°C, C_{N_f} = 2.0 g N dm^{-3}. Bobieritte appeared only under one condition (pH 10.0, 20.0 °C, and C_{N_f} = 1.0 g N dm^{-3}), where it accounted for 8.5 % of the precipitated product.

Under extreme conditions (pH 10.0, 50.0°C), the undefined phase ($p_{undefined\ phase}$) accounted for at least 20.0 % of the recovered product, regardless of the feed composition. The poorest quality product, composed of 60.0 % undefined phase and 40.0 % brucite, was obtained under the same extreme tested conditions (pH 10.0, 50.0°C), and high feed concentration (C_{N_f} = 3.0 g N dm^{-3}), where the product consisted of 60.0 % undefined phase and 40.0 % brucite.

Struvite purity ($p_{struvite}$) was moderately influenced by pH (R^2 = 0.3; Figure S2a), whereas, within the temperature range tested and under the provided excess of ammonium (N:P = 2.5), no significant effect of T on struvite purity was observed (R^2 = 0.1; data not shown). However, in systems with a lower initial N:P ratio, the influence of temperature on NH_4^+ availability would have a more pronounced effect on struvite crystallization and purity. In contrast, the formation of struvite admixtures increased with pH. For example, cattiite formation was moderately correlated with pH (R^2 = 0.4; Figure S2b), while brucite, bobierrite, and undefined phases showed only a marginal pH dependence (R^2 = 0.1). Brucite precipitation also exhibited a weak positive correlation with feed concentration (R^2 = 0.2; Figure S2c).

These findings highlight the importance of maintaining slightly alkaline pH (8.0–9.0) and controlling feed concentrations to optimize struvite purity and minimize co-precipitation of less desirable products.

3.1.2. Effect on P recovery

Phosphorus recovery was evaluated based on reconciled results derived from two independent measurement methods: XRF and cuvette-based colorimetric testing. Equal weights ($w_1 = w_2 = 0.5$) were applied in the data reconciliation procedure to obtain a unified estimate of P recovery. Reconciled results are presented in Table S5, while mass balance-based values for ηP_{REC}, $\eta P_{struvite}$, and $\eta P_{other\ form}$ are summarized in Table S6.

Across the tested operational conditions, ηP_{REC} ranged from 38.2 % (pH 9.0, 10.0 °C, C_{N_f} = 2.0 g N dm^{-3}) to 99.3 % (pH 7.3, 35.0

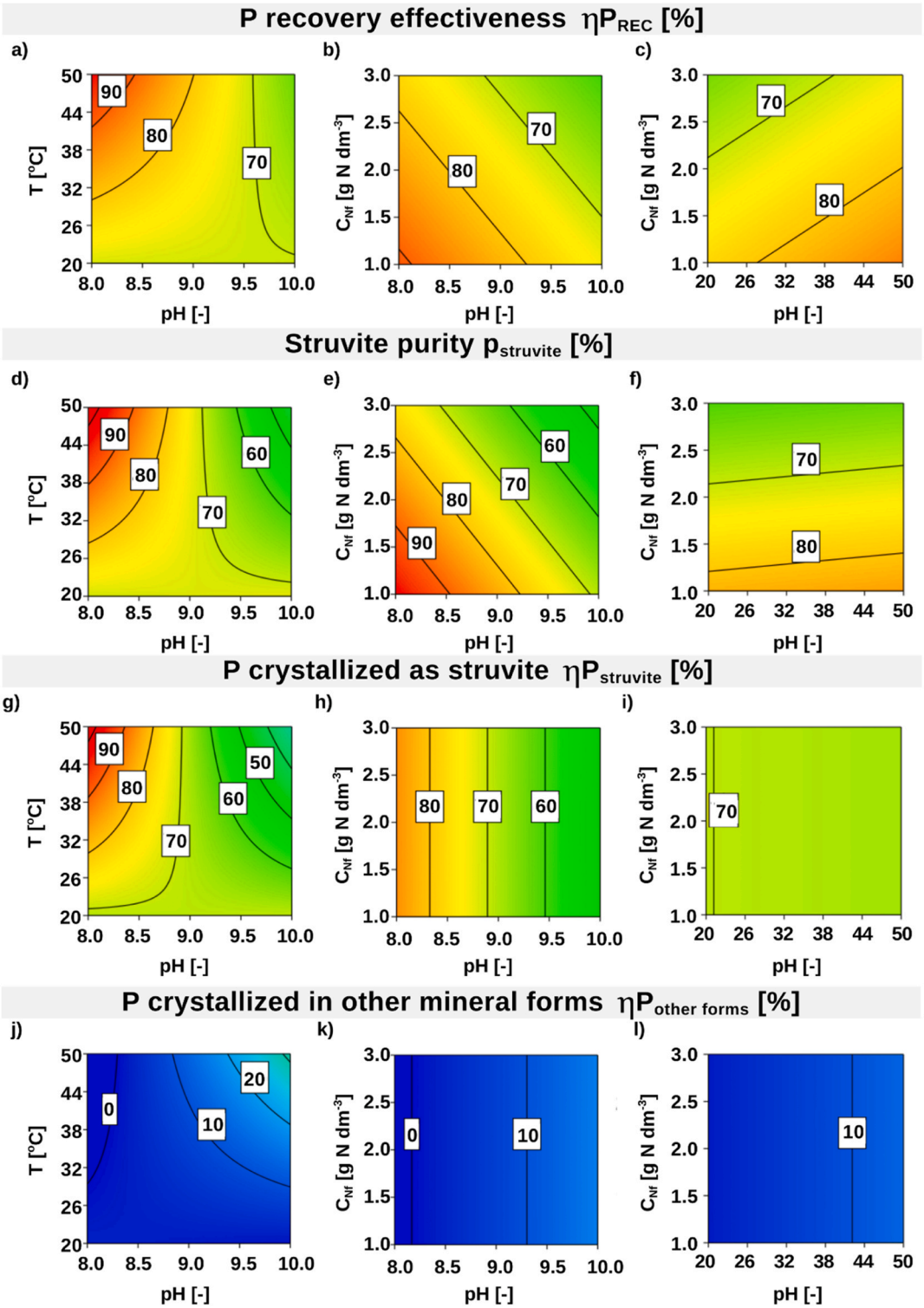

Fig. 4. Effect of the operational parameters on the recovered product composition and P removal and recovery pathways in the integrated struvite precipitation and GLMS process: a) ηP_{REC} (pH, T); b) ηP_{REC} (pH, C_{N_f}); c) ηP_{REC} (T, C_{N_f}); d) $p_{struvite}$ (pH, T); e) $p_{struvite}$ (pH, C_{N_f}); f) $p_{struvite}$ (T, C_{N_f}); g) $\eta P_{struvite}$ (pH, T); h) $\eta P_{struvite}$ (pH, C_{N_f}); i) $\eta P_{struvite}$ (T, C_{N_f}); j) $\eta P_{other\ forms}$ (pH, T); k) $\eta P_{other\ forms}$ (pH, C_{N_f}); l) $\eta P_{other\ forms}$ (T, C_{N_f}).

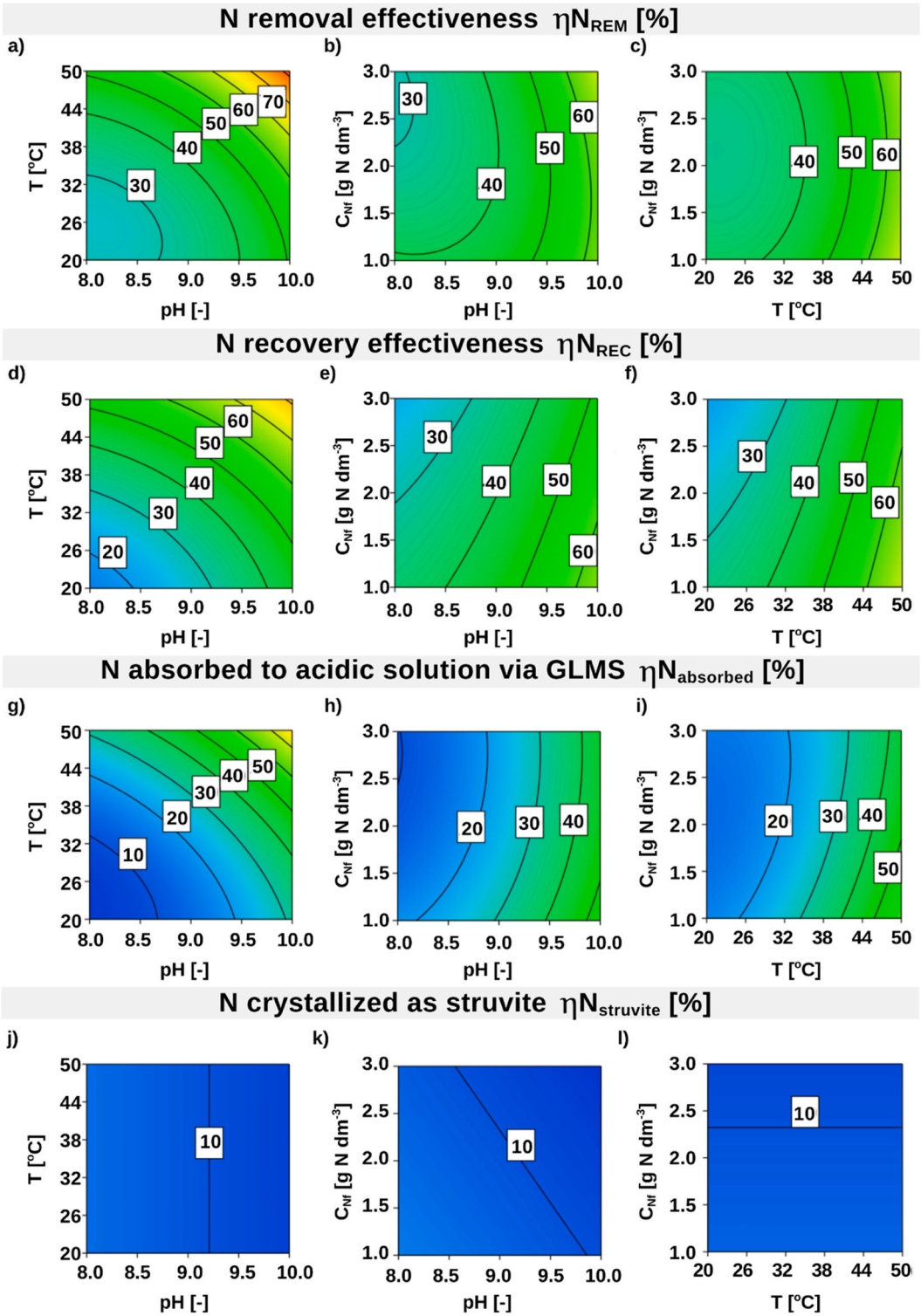

Fig. 5. Effect of the operational parameters on N removal and recovery pathways in the integrated struvite precipitation and GLMS process: a) ηN_{REM} (pH, T); b) ηN_{REM} (pH, C_{N_f}); c) ηN_{REM} (T, C_{N_f}); d) ηN_{REC} (pH, T); e) ηN_{REC} (pH, C_{N_f}); f) ηN_{REC} (T, C_{N_f}); g) $\eta N_{absorbed}$ (pH, T); h) $\eta N_{absorbed}$ (pH, C_{N_f}); i) $\eta N_{absorbed}$ (T, C_{N_f}); j) $\eta N_{struvite}$ (pH, T); k) $\eta N_{struvite}$ (pH, C_{N_f}); l) $\eta N_{struvite}$ (T, C_{N_f}).

°C, same feed composition). These values correspond to the lowest investigated levels of T and pH. The average ηP_{REC} achieved 75.5 ± 16.9 %.

At pH ≤ 9.0, the recovered precipitate contained only struvite as the P-containing product. At higher pH, additional crystalline phosphate phases appeared. The $\eta P_{other\ form}$ values ranged from 1.9 % (pH 10.0, 20.0 °C, $C_{N_f} = 3.0$ g N dm^{-3}) to 60.0 % (pH 10.0, 50.0 °C, same feed composition), indicating a significant shift toward formation of secondary P forms under highly alkaline and thermal conditions. A moderate negative correlation was found between pH and both ηP_{REC} ($R^2 = 0.2$) and $\eta P_{struvite}$ ($R^2 = 0.4$), while $\eta P_{other\ form}$ increased with pH ($R^2 = 0.3$) (Figure S2d-**f**). T and feed composition showed minimal or no effect ($R^2 \leq 0.1$) on ηP_{REC} and $\eta P_{other\ form}$, although the formation of non-struvite forms was most pronounced under extreme conditions (pH 10.0, 50.0 °C).

3.1.3. Effect on N removal

Mass balance-based ηN_{REM} results, along with ηN_{REC} and ηN_{loss}, are presented in Table S6**.** The overall ηN_{REM} was positively influenced by increasing pH and T, with moderate correlations (R^2 of 0.4) (Figure S2 **g-h**). No significant relationship was observed between ηN_{REM} and feed concentration. Similar were observed for ηN_{REC}, which was moderately correlated with both pH ($R^2 = 0.3$) and T ($R^2 = 0.5$) (Figure S2 **i-j**), indicating that N recovery was the dominant N removal pathway across the tested conditions.

On average, ηN_{loss} was low at 9.3 ± 8.5 %, and showed no dependency on pH and T. However, N loss increased significantly with rising feed N concentration, with an R^2 of 0.3 (Figure S2 **k**). The highest ηN_{loss} (28.6 %) coincided with the highest ηN_{REM} (96.1 %) under the most extreme tested condition (pH 10.0, 50.0 °C, $C_{N_f} = 3.0$ g N dm^{-3}). In contrast, the lowest ηN_{REM} (23.2 %) and no N loss ($\eta N_{loss} = 0.0$ %) occurred at pH 7.3, 35.0 °C and $C_{N_f} = 2.0$ g N dm^{-3}.

The ηN_{REC} values ranged from 17.4 % (pH 8.0, 20.0 °C, $C_{N_f} = 3.0$ g N dm^{-3}) to 93.1 % (pH 10.0, 50.0 °C, $C_{N_f} = 1.0$ g N dm^{-3}). Across the investigated range of pH, T and feed composition, the average ηN_{REC} reached 47.6 ± 23.4 %. However, the dominant N recovery pathway (struvite crystallization vs. NH_3 absorption) depended on the applied operational conditions.

3.1.4. Effect on N recovery

Detailed ηN_{REC} results, along with $\eta N_{struvite}$ and $\eta N_{absorbed}$, are presented in Table S6. Integrating struvite precipitation and GLMS enhanced N recovery effectiveness regardless of the applied operational conditions. On average, $\eta N_{struvite}$ was only 10.7 ± 5.2 %, while $\eta N_{absorbed}$ contributed 37.0 ± 24.6 %. The $\eta N_{struvite}$ values ranged from 0.0 % (pH 10.0, 50.0 °C, $C_{N_f} = 3.0$ g N dm^{-3}) to 16.8 % (pH 9.0, 35.0 °C, $C_{N_f} = 2.0$ g N dm^{-3}), while $\eta N_{absorbed}$ varied from 6.5 % (pH 7.3, 35.0 °C, same feed composition) to 89.0 % (pH 10.0, 50.0 °C, $C_{N_f} = 1.0$ g N dm^{-3}).

Struvite-based N recovery ($\eta N_{struvite}$) was independent of T, but decreased with increasing pH ($R^2 = 0.3$; Figure S2 **l**) and feed concentrations ($R^2 = 0.1$; data not shown). In contrast, $\eta N_{absorbed}$ was strongly influenced by both pH and T increase ($R^2 = 0.4$) (Figure S2 **m-n**), in line with enhanced NH_3 volatilization (Serra-Toro et al., 2022). These findings confirm that struvite precipitation and GLMS are complementary techniques. While struvite precipitation facilitates NH_4^+ immobilization, GLMS enables effective NH_3 absorption, together enabling comprehensive N valorization.

3.2. Development of RSM-based predictive models

Full quadratic RSM-based models were developed based on the experimental data to describe the performance of the integrated struvite precipitation and GLMS system. The models predicted $\eta P_{struvite}$, $\eta P_{other\ form}$, ηP_{REC}, $p_{struvite}$, ηN_{REM}, ηN_{REC}, $\eta N_{absorbed}$, $\eta N_{struvite}$ and ηN_{loss} as described by Eqs S1-S9. Overall, the models demonstrated high predictive performance, with $R^2 = 1.0$ for ηN_{REC} and $\eta N_{absorbed}$, 0.9 for ηN_{REM}, 0.7 for $\eta P_{struvite}$, $\eta P_{other\ form}$, ηP_{REC}, $p_{struvite}$, and 0.6 for $\eta N_{struvite}$ and ηN_{loss} (Table S7).

Statistical analysis confirmed that all three variables (pH, T, feed concentration) influenced system performance. Among these, pH showed the strongest and most consistent effect (p-value ≤ 0.2), significantly affecting all predicted outcomes (Table S8). Feed concentration was statistically significant for all outputs except $\eta P_{struvite}$ and $\eta P_{other\ form}$, while the effect of T had no significant effect on $\eta N_{struvite}$ and ηN_{loss}. Furthermore, pH-T, pH-C_{N_f}, and T-C_{N_f} interaction terms also contributed to model outcomes. A pH-T interaction significantly influenced $\eta P_{struvite}$, $\eta P_{other\ form}$, ηP_{REC}, $p_{struvite}$, ηN_{REM} and $\eta N_{absorbed}$. A pH-C_{N_f} interaction was found for ηN_{REM} and ηN_{loss}. Finally, a T-C_{N_f} interaction was observed for $\eta N_{absorbed}$.

Simplified models for all the outcomes were developed based on the statistical significance of variables (Eqs S10-S18). The simplified models retained strong predictive capability, with no loss in accuracy for ηN_{REM} and $\eta N_{absorbed}$, and only a slight decrease ($\Delta R^2 = 0.1$) for the remaining outputs (Table S7), confirming the robustness of the simplification process. Contour plots derived from the simplified models illustrate the interactive effects of pH-T, pH-C_{N_f} and T-C_{N_f} on system performance, including ηP_{REC}, $p_{struvite}$, $\eta P_{struvite}$, $\eta P_{other\ forms}$ (Fig. 4**a-l**), ηN_{REM}, ηN_{REC}, $\eta N_{struvite}$, $\eta N_{absorbed}$ (Fig. 5**a-l**), and on ηN_{loss} (Figure S3a-**c**).

At pH < 9.0, T > 30.0 °C and $C_{N_f} < 2.5$ g N dm^{-3}, ηP_{REC} exceeded 80.0 %. A strong interaction between pH and T was observed under pH < 9.5, while this effect diminished at higher pH levels (Fig. 4**a**). The ηP_{REC} values also increased linearly with decreasing pH and C_{N_f}, and with increasing T (Fig. 4**b-c**). Similar trends were observed for $p_{struvite}$. However, struvite purity showed a higher sensitivity than P recovery efficiency to increasing pH (>9.0) and C_{N_f} (>1.0 g N dm^{-3}) (Fig. 4**d–f**). At T < 30.0 °C, the pH-T interaction had limited influence on $p_{struvite}$ (Fig. 4 **a**) and thus P recovery form, showing a decrease in $\eta P_{struvite}$ (Fig. 4**g**) in favour of $\eta P_{other\ form}$ (Fig. 4**j**). However, at higher T, struvite purity increased notably with decreasing pH, with $p_{struvite}$ exceeding 90.0 % at pH < 8.2. This suggests that slightly alkaline combined with elevated T favors selective struvite formation over competing precipitate forms. Additionally, higher feed concentrations negatively affected product purity. High C_{N_f} along with elevated pH and T levels may shift the crystallization pathway toward less homogenous forms (Fig. 4**e-f**). Nevertheless, C_{N_f} alone exerted a negligible influence on the

efficiency of P precipitation, whether as struvite or as other phosphate forms (Fig. 4**h–j, k–l**).

A clear pH-T interaction was also observed for ηN_{REM}, particularly at pH > 9.0 and T > 40.0 °C, where the influence of C_{N_f} became negligible (Fig. 5**a-c**). Similar trends were found for ηN_{REC} (Fig. 5**d-f**) and $\eta N_{absorbed}$ (Fig. 5**g-i**), indicating that elevated pH and T are the dominant factors driving NH_3 volatilization and subsequent absorption. In contrast, $\eta N_{struvite}$ was T-independent (Fig. 5**j,l**) and was mostly influenced by a C_{N_f}–pH interaction (Fig. 5**k**), closely aligning with the trends observed for $p_{struvite}$ (Fig. 4**e**) and $\eta P_{struvite}$ (Fig. 4**h**), confirming the dependence of struvite precipitation on both nutrient availability and crystallization conditions. Finally, a notable interaction between pH and C_{N_f} was identified also for ηN_{loss} (Figure S3b). At pH > 8.5, ηN_{loss} decreased with increasing pH under dilute conditions (C_{N_f} <1.5 g N dm^{-3}). However, under concentrated feed conditions, increasing pH led to higher NH_3 losses, highlighting the risk of excessive NH_3 volatilization under high nutrient loads, independently of T (Figure S3a**,c**).

3.3. Process optimization results

The results of the optimization Scenario 1, which aimed to maximize both ηN_{REC} and ηP_{REC} without imposing constraints on the operational parameters, showed pH 9.5 and 50.0°C as the optimal operational conditions, regardless of the feed concentrations. However, these concentrations had a moderate effect on recovery effectiveness (ηN_{REC} and ηP_{REC}). As C_{N_f} and C_{P_f} increased within the tested range (1.0–3.0 g N dm^{-3} and 0.4–1.2 g P dm^{-3}, respectively) both ηN_{REC} and ηP_{REC} decreased by approximately 13 %, from 78.7 % to 64.8 % and from 77.1 % to 64.5 %, respectively (Table 2).

In Scenario 2, where additional constrains were imposed to minimize pH and T, the optimized conditions shifted to pH 8.0 and 40.7 °C. These changes resulted in a significant reduction in ηN_{REC} (to 43.4 %) caused by reduced NH_3 stripping, but a notable increase in ηP_{REC} (from 77.1 % to 95.7 %) and struvite purity ($p_{struvite}$ from 68.2 % to 100.0 %) due to enhanced NH_4^+ availability for struvite precipitation compared to Scenario 1. Similar to Scenario 1, the increased feed concentrations led to reduced recovery effectiveness, with ηN_{REC} and ηP_{REC} decreasing to 33.9 % and 84.1 %, respectively.

Although 100 % $p_{struvite}$ was already achieved in Scenario 2, prioritizing struvite purity over ηN_{REC} and ηP_{REC} effectiveness was investigated in Scenario 3. This approach yielded an optimal T of 38.4 °C (reduction by 2.0 °C), with only a modest reduction of 2.0–3.0 % in ηP_{REC} and ηN_{REC}.

4. Discussion

4.1. Integration feasibility and mutual interactions between struvite precipitation and GLMS

This study demonstrates the technical feasibility of integrating struvite precipitation and GLMS into a single-stage system for nutrient recovery from N and P rich streams, such as anaerobic digester liquors. The inclusion of suspended GPM resulted in a threefold increase in ηN_{REC} compared to struvite precipitation alone.

Operational conditions, including pH, T and feed concentration, played a central role in balancing nutrient recovery pathways and determining the forms of recovered products. A key trade-off emerged from the interaction between NH_3 volatilization (for GLMS) and NH_4^+ availability (for struvite). At $[NH_3] \geq 80$ %, an increase in $\eta N_{absorbed}$ corresponded to a decrease in $\eta P_{struvite}$ (Figure S4 **a–b**). This inverse relationship is attributed to NH_4^+ depletion in the solution, which is a critical ion for struvite precipitation at a fixed NH_4^+:PO_4^{3-} molar ratio of 1.0 (Guan et al., 2023). In the tested lab-scale conditions, the synthetic feed solution was prepared ensuring an excess of ammonium relative to phosphate with an initial molar ratio of 2.5. However, in real wastewaters, NH_4^+:PO_4^{3-} molar ratios may vary widely depending on the source, treatment stage, and upstream processes (Achilleos et al., 2022). If the NH_4^+:PO_4^{3-} molar ratio falls below 1.0 (which accounts to mass ratio of 0.20), struvite formation can be significantly hindered, and the negative effect of NH_3 stripping becomes more pronounced to struvite formation (Fig. 6). Therefore, in practical applications, particularly in streams where NH_4^+ is not present in sufficient excess to sustain simultaneous NH_3 stripping and struvite precipitation, the integrated system performance may differ.

Although the tightly sealed reactor design, ηN_{loss} was not completely avoided. The observed losses were likely caused by NH_3 entrainment in water vapor, which can hinder its transfer to the absorbent through hydrophobic GPMs (Palakodeti et al., 2021).

Despite these challenges, the system was able to produce two valuable fertilizers simultaneously: crystalline struvite and $(NH_4)_2SO_4$ solution (Śniatała et al., 2024). This dual-recovery approach fits well with the objectives of modern resource recovery-oriented wastewater treatment and supports regulations promoting nutrient valorization, such as the new Urban Wastewater Directive (EU 2024/3019).

Unlike conventional multi-stage systems, the proposed compact reactor design eliminates the need for intermediate connections

Table 2
Summary of optimization results for Scenarios 1-3.

	Operational parameters			Output parameters		
	pH [-]	**T [°C]**	**C_{N_f} [g N dm^{-3}]**	**ηP_{REC} [%]**	**ηN_{REC} [%]**	**$p_{struvite}$ [%]**
Scenario 1	9.5	50.0	1.0	77.1	78.7	68.2
Scenario 2	8.0	40.7	1.0	95.7	43.4	100.0
Scenario 3	8.0	38.4	1.0	93.7	40.2	100.0

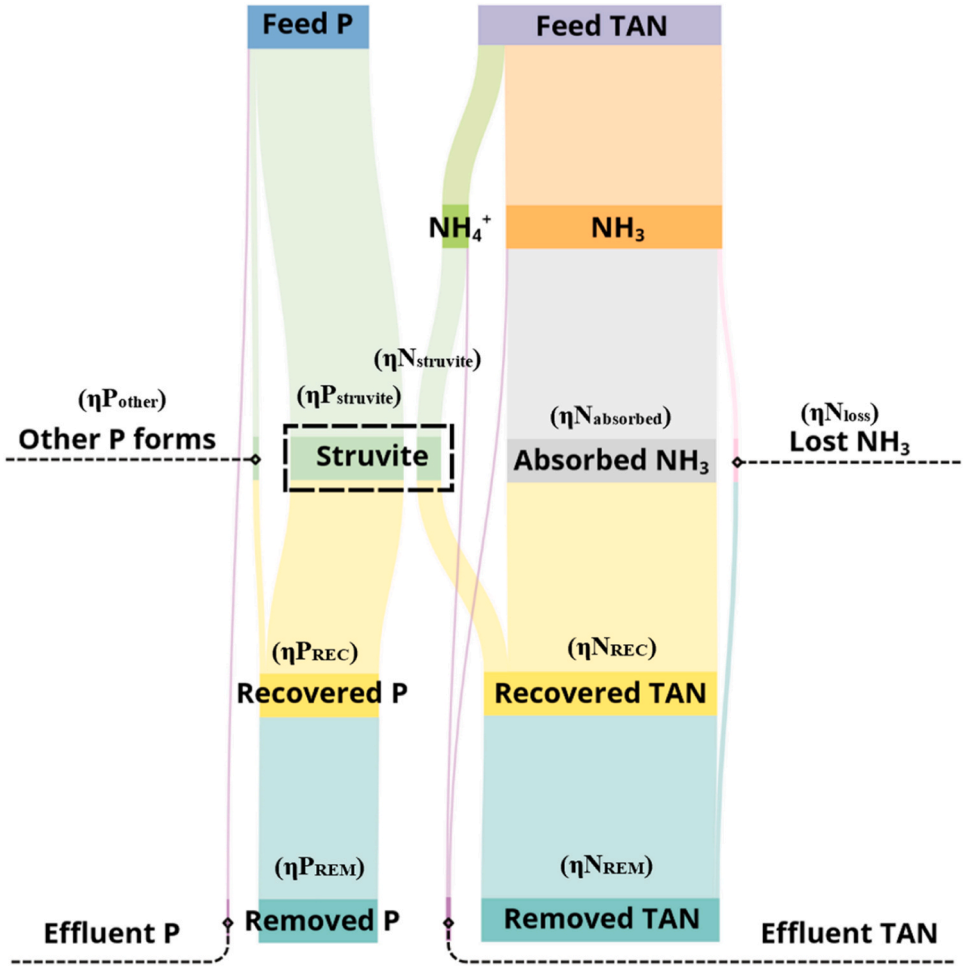

Fig. 6. Detailed visual representation of N and P mass flow in the single-stage P precipitation and NH_3-oriented GLMS process.

between separate units, thereby overcoming limitations related to spatial footprint, energy consumption and process complexity (Wu and Vaneeckhaute, 2022). Simplified operation can further be enabled by the use of $Mg(OH)_2$, which serves as both a pH regulator and Mg^{2+} source (Hollas et al., 2021). However, the low solubility of $Mg(OH)_2$ can occasionally limit Mg^{2+} availability, especially under low T, leading to $Mg(OH)_2$ co-precipitation and reduced struvite purity (Yu et al., 2013).

4.2. Recovered products quality and valorization potential

4.2.1. Struvite

The integrated system achieved P recovery of up to 1.02 kg P per 1 m^{-3} of feed solution, which is comparable to yields reported for other integrated N and P recovery technologies (Cao et al., 2019; Tian et al., 2019). However, pure struvite ($p_{struvite}$ = 100.0 %) was only obtained under specific conditions: pH 8.0, 50.0 °C, and C_{N_f} = 1.0 g N dm^{-3}.

The presence of co-precipitating P forms in struvite can affect product purity, its bioavailability, and fertilizing properties (Śniatała et al., 2024). In the controlled laboratory experiments, the feed solution contained only PO_4^{3-}, NH_4^+, Mg^{2+}, sodium (Na^{2+}), H^+, and hydroxide (OH^-) ions. Among these, Mg^{2+} and Na^{2+} are known to compete during the crystallization process (Hollas et al., 2021). However, the presence of Na^{2+} was only associated with products that also contained significant amounts of undefined crystalline phases, mainly observed at pH 10.0 and 50.0°C.

High pH and elevated T ($\geq$ 50.0°C) are known to promote the formation of struvite co-precipitating products (Capdevielle et al., 2016; Tansel et al., 2018). Under such conditions, NH_4^+ ions are converted into free NH_3, reducing their availability for struvite formation (Krishnamoorthy et al., 2021). This shift can lead to acidification of the solution and favor the precipitation of competing phases, such as amorphous magnesium phosphate ($Mg_3(PO_4)_2$), Na• salts formed through partial substitution of NH_4• or brucite (Ha et al., 2024; Hao et al., 2013; Zhou et al., 2024). In the present study, the lowest product quality was observed at pH 10.0 and 50.0 °C, with the precipitate consisting of 60.0 % undefined phase and 40.0 % brucite.

The dependence of struvite purity on solution pH and ion content is well explained by supersaturation theory, as the solubility of

Table 3
Economic analysis of reported physicochemical single-stage integrated N and P recovery technologies.

Technology		Operational conditions	Energy		Chemicals		Products and their market value		Total cost (USD/ $kgN_{removed}$) **	Total revenue (USD/ $kgN_{removed}$) ****	Reference
			Consumption (kWh/ $kgN_{removed}$)	**Cost (USD/ $kgN_{removed}$) ***	**Consumption (kg/$kgN_{removed}$)**	**Cost (USD/ $kgN_{removed}$) ***	**Type and amount**	**Revenue (USD/ $kgN_{removed}$) ****			
Struvite precipitation and GLMS	**Scenario 1)**	pH = 9.5 T = 50.0 °C C_{N_f} = 1.0 g N dm^{-3} C_{P_f} = 0.4 g P dm^{-3} Mg:P = 1.5 N:P = 2.5	21.8	6.76	4.0 kg H_2SO_4 1.4 kg $Mg(OH)_2$ 4.0 kg NaOH	2.66	- Struvite (0.4 kg P) - $(NH_4)_2SO_4$ (0.9 kg N)	6.62	9.42	-2.80	This study
	Scenario 2)	pH = 8.0 T = 40.7 °C C_{N_f} = 1.0 g N dm^{-3} C_{P_f} = 0.4 g P dm^{-3} Mg:P = 1.5 N:P = 2.5	14.5	4.48	4.0 kg H_2SO_4 1.4 kg $Mg(OH)_2$ 0.2 kg NaOH	1.52	- Struvite (0.8 kg P) - $(NH_4)_2SO_4$ (0.5 kg N)	12.82	6.00	6.82	
	Scenario 3)	pH = 8.0 T = 38.4 °C C_{N_f} = 1.0 g N dm^{-3} C_{P_f} = 0.4 g P dm^{-3} Mg:P = 1.5 N:P = 2.5	9.2	2.86	4.0 kg H_2SO_4 1.4 kg $Mg(OH)_2$	1.52	- Struvite (0.8 kg P) - $(NH_4)_2SO_4$ (0.5 kg N)	13.20	4.37	8.83	
Struvite precipitation and NH_3 air stripping		pH = 9.0-10.0 T = 40.0 °C C_{N_f} = 0.3 g N dm^{-3} C_{P_f} = 0.1 g P dm^{-3} Mg:P = 6.6 N:P = 6.6	79.2	24.55	MgO: 5.5 H_3PO_4: 2.1	5.21	- Struvite (0.1 kgP) - $NH_4H_2PO_4$ (1) kg P)	1.5 29.75		-28.26	(Cao et al., 2019)
P precipitation and LLMS		pH = 12.0 T = 30.0 °C C_{N_f} = 3.9 g N dm^{-3} C_{P_f} = 0.2 g P dm^{-3} Ca:P = 19.0 N:P = 43.0	18.5	5.73	5.1 kg H_2SO_4 4.8 kg $Ca(OH)_2$	1.33	- Hydroxyapatite (0.01 kg P) - $(NH_4)_2SO_4$ (1.3 kg N) - $CaCO_3$ (6.2 kg)	9.29	7.07	2.22	(Pradhan et al., 2019)
Struvite precipitation and VTS		pH = 9.1 T = 60.0 °C C_{N_f} = 5.1 g N	8.0	2.50	4.0 kg H_2SO_4 0.5 kg $MgCl_2 \cdot 6 H_2O$	0.78	- Struvite (0.1 kg P)	18.02	3.28	14.74	(Tian et al., 2019)

(*continued on next page*)

Table 3 (*continued*)

Technology	Operational conditions	Energy		Chemicals		Products and their market value		Total cost (USD/ $kgN_{removed}$) **	Total revenue (USD/ $kgN_{removed}$) ****	Reference
		Consumption (kWh/ $kgN_{removed}$)	**Cost (USD/ $kgN_{removed}$)** *	**Consumption (kg/$kgN_{removed}$)**	**Cost (USD/ $kgN_{removed}$)** *	**Type and amount**	**Revenue (USD/ $kgN_{removed}$)** **			
	dm^{-3} C_{P_i} = 0.3 g P dm^{-3} Mg:P = 1.1 N:P = 37.6					- $(NH_4)_2SO_4$ (2.1 kg N)				

* market prices given in Table S9;** calculated based on the nutrient content in the recovered products including their market process presented in Table S9; *** sum of energy and chemicals cost; **** calculated as difference between total cost and revenue from recovered products.

Mg^{2+}, PO_4^{3-} and NH_4^+ is highly sensitive to pH (Le et al., 2024; Tansel et al., 2018). The optimal pH for struvite formation was found to be $\leq$ 8.6 for high struvite purity, which is consistent with previous studies (Daneshgar et al., 2022; Günther et al., 2018).

Minor admixtures, such as cattiite ($Mg_3(PO_4)_2$22 H_2O), tend to form at pH > 10.0 (Lecorre et al., 2007). In the present study, cattiite crystals were detected at pH 9.0 – 10.0, constituing less than 10 % of the solid product. Although cattiite can easily convert to bobierrite ($Mg_3(PO_4)_2$·8 H_2O) in the aqueous phase (Bhuiyan et al., 2008; Sun et al., 2023), bobierrite was only found in the dried sample precipitated from the solution containing 1.0 g N dm^{-3} and 0.4 g P dm^{-3} at pH of 10.0 and 20.0°C. Brucite was also commonly present in the precipitate, likely due to limited solubility of $Mg(OH)_2$. Incomplete dissolution of $Mg(OH)_2$ may not match the kinetics of PO_4^{3-} and NH_4^+ release, especially at lower T, which can reduce struvite formation and increase the need for additional Mg^{2+} input (Krishnamoorthy et al., 2021; Tansel et al., 2018).

Although pH is a key factor influencing solution supersaturation and crystallization kinetics (Guan et al., 2023; Le Corre et al., 2009), its optimal value can vary depending on wastewater characteristics, including T, Mg:P:N molar ratio, and the presence of competing ions or organic matter (Krishnamoorthy et al., 2021; Yan et al., 2025).

4.2.2. $(NH_4)_2SO_4$

For liquid $(NH_4)_2SO_4$ fertilizer, the N concentration is a key measure of product quality. Commercial $(NH_4)_2SO_4$ solutions typically contain between 20.0 and 26.0 g N dm^{-3} and maintain a strong acidic pH (approximately 2.0) (Rodrigues et al., 2022; Śniatała et al., 2024). In the present study, the N concentration in the recovered product was significantly lower, reaching only 2.02 g N dm^{-3} at pH 10.0 and 50.0°C, at the highest N loading (C_{N_f} = 3 g N dm^{-3}). Previous studies have demonstrated that the final N concentration can be increased by adjusting the volume (V_a) and molarity of the absorbent solution (Amaral et al., 2016).

In addition to the absorbent characteristics, the temperature gradient between the feed and the absorbent solution (ΔT) also affected mass transfer and dilution in the recovered solution. At ΔT = 35.0 °C (with the feed T = 60.0 °C), V_a increased by approximately 10.0 %, likely due to water vapor permeating through the membrane. However, elevated feed T also increased $\eta N_{absorbed}$. In contrast, when the temperature gradient was reversed (ΔT = -15.0°C, with the feed T = 10.0°C), V_a decreased by approximately 4.0 %. These findings indicate that reducing ΔT can enhance $(NH_4)_2SO_4$ concentration in the recovered solution, leading to a higher quality of the final product (Yang and Qin, 2024). Therefore, careful control of the absorbent T, either through passive management or active heating, can improve process effectiveness.

Although GLMS systems are designed to prevent a direct contact between the membrane and the feed, trace amounts of other volatile compounds can be detected in the permeate stream. Luqmani et al. (2024) identified the presence of volatile organic compounds (VOCs) in the permeate alongside NH_3 and water vapor. The detection of these compounds may restrict the direct reuse of the recovered solution in applications that require high purity products (Vaneeckhaute et al., 2017). Despite this, GLMS offers the advantage of separating nutrient recovery from direct feed contact, which reduces a risk of membrane fouling (Zhu et al., 2024). However, an optimal balance between the total mass transfer and NH_3 selectivity is essential to achieve both high recovery efficiency and product quality (Luqmani et al., 2024; Śniatała et al., 2024).

4.3. Comparison to other single-stage physicochemical N and P recovery technologies

To highlight the strengths and weaknesses arising from energy and chemical consumption, as well as from the nutrient concentrations in the recovered products, a preliminary theoretical economic comparison of available single-stage physicochemical N and P recovery technologies was developed, following the assumptions and methodologies reported in literature (Cao et al., 2019; Pradhan et al., 2019; Tian et al., 2019).

Regardless of the optimization scenario (1−3), treating mesophilic anaerobic digestion liquors (35 °C, near-neutral pH) containing 1 g N dm^{-3} using our technology requires baseline inputs of 0.3 kWh for pumping, 4.0 kg H_2SO_4, (absorbent) and 1.4 kg $Mg(OH)_2$ per kg N removed (Table 3). These correspond to fixed chemical and energy costs of approximately 1.61 USD/kg $N_{removed}$ (based on prices presented in Table S9).

The integrated system achieved high recovery effectiveness in laboratory experiments (ηP_{REC} = 98.8 %, ηN_{REC} = 93.1 %), but these peaks occurred under different and energy-intensive conditions. The highest ηN_{REC} was observed at pH 10.0 and 50.0 °C, while ηP_{REC} peaked at pH 7.3 and 35.0 °C. Scenario 1 tried to balance both conditions, achieving approximately 80.0 % recovery of both N and P, but this resulted in higher operational costs due to the energy demand for heating and chemical usage (9.42 USD/kg $N_{removed}$ (Table 3)), generating a net deficit of −2.80 USD/kg $N_{removed}$. In contrast, Scenarios 2 and 3 showed that operating under more moderate conditions (pH 8.0, 38.4–40.7 °C) reduced the costs significantly (6.00 and 4.37 USD/kg $N_{removed}$, respectively) and offered the total process revenue of 6.82 and 8.83 USD/kg $N_{removed}$, respectively. Moreover, Scenario 3 produced struvite of very high purity. This high quality product could help with its certification and marketability (Santos et al., 2024). These results suggest that full-scale implementation should be adapted to the local operating conditions and goals of each WWTP, considering process flexibility and energy efficiency. Nevertheless, regardless of the chosen scenario, the proposed system offers a modular and compact solution that supports the transition to a circular economy in the wastewater sector and facilitates compliance with emerging EU regulations (EU 2024/, 3019). However, rigorous economic analyses should be undertaken only after the technology has been sufficiently upscaled and its performance validated under real operational conditions.

Comparison of available single-stage physicochemical N and P recovery technologies, highlighted air stripping as the least energetically and economically efficient N recovery approach. Despite its integration with struvite precipitation in one reactor, removal of 1.0 kg N from digested swine wastewater (C_{N_f} = 0.3 g N dm^{-3}, C_{P_f} = 0.1 g P) consumed 79.22 kWh/kg (Cao et al., 2019), which is at least 4 times higher compared to other single-stage integrated technologies. Although 88.0 % N and 96.1 % P were recovered by

precipitation of struvite and NH_3 absorption to phosphoric acid (H_3PO_4), the final product contained only 0.1 kg P, which together with high energy and chemicals consumption (5.5 kg of magnesium oxide (MgO) acting as struvite precipitation agent and pH control, and 2.1 kg H_3PO_4) resulted in a deficit of −28.26 USD/kg $N_{removed}$.

In contrast, the least chemically and energetically intensive was integrated struvite precipitation and vacuum thermal stripping (VTS) reported by Tian et al. (2019). This process, without pH adjustment at 60.0 °C and 21.3 kPa recovered 0.5 kg/kg $N_{removed}$ of struvite containing 0.1 kg P and 10.1 kg/kg $N_{removed}$ $(NH_4)_2SO_4$ with 2.1 kg N from hydrolyzed urine (C_{N_f} = 5.1 g N dm^{-3}, C_{P_f} = 0.3 g P dm^{-3}) offering revenue of 14.74 USD/kg $N_{removed}$. The high nutrient concentration in the feed reduced the energy required for heating, as only 0.25 m^3 of hydrolyzed urine had to be heated from room temperature to 60.0 °C to remove 1 kg of N, which consumed only 7.1 kWh.

Finally, Pradhan et al. (2019) reported harvesting of $(NH_4)_2SO_4$ containing 1.3 kg N and calcium phosphate (hydroxyapatite, $Ca_{10}(PO_4)_6(OH)_2$) with 0.01 kg P from urine (C_{N_f} = 3.9 g N dm^{-3}, C_{P_f} = 0.2 g P dm^{-3}, N:P = 43.0) at pH 12.0 and 30.0 °C using P chemical precipitation and LLMS. The method used calcium hydroxide ($Ca(OH)_2$); Ca:P = 19.0) to increase the feed pH and simultaneously precipitate P. From 1 kg $N_{removed}$, the harvested $(NH_4)_2SO_4$ contained 1.3 kg N and struvite 0.01 kg P. Moreover, calcium carbonate ($CaCO_3$; 6.2 kg) was recovered. The extraction of N and P from could give a profit of 2.22 USD/kg $N_{removed}$, which is 3 and 4 times less compared to our technology operating according to optimization scenarios 2 and 3, respectively. Moreover, GLMS application instead of LLMS enabled eliminating problems associated with GPM clogging (Soto-Herranz et al., 2021).

5. Future outlook

The proposed integration of struvite precipitation and GLMS into one system shows promising results for combined N and P recovery. However, several areas need more research to improve technical strength and economic feasibility in full-scale applications.

Regarding process development, future research should optimize T gradients between the feed and absorbent to improve ammonia–water selectivity in GLMS (Yang and Qin, 2024). Controlled studies are also needed to assess how the feed N:P molar ratio impacts precipitation pathways and product purity, especially with varying wastewater characteristics, (Wu and Vaneeckhaute, 2022). Additionally, testing alternative dual-function Mg^{2+} sources with better solubility, such as $MgHPO_4{\cdot}3H_2O$ wrapped with $Mg(OH)_2$ (Zhou et al., 2024), may improve control of feed solution supersaturation and reduce co-precipitation of brucite, thus enhancing struvite quality. Moreover, a comprehensive analysis of precipitate morphology and elemental composition using scanning electron microscopy with energy-dispersive X-ray spectroscopy (SEM-EDS) is recommended to fully characterize the crystallized products and validate their stoichiometry.

For the mass balance validation, direct NH_3 measurements in the gas phase are needed to verify the assumptions for GLMS, especially for estimating ηN_{loss}. This is important for better understanding the process kinetics and optimizing the HRT, and the absorbent volume and molarity. This is particularly important if the technology is applied to anaerobic digester liquors or other high-strength wastewaters containing various volatile compounds.

It should be noted that this study was conducted using synthetic wastewater. The absence of competing ions, heavy metals, and organic matter, which are typical in real anaerobic sludge digestion liquors, likely contributed to the observed high nutrient recovery effectiveness and product purity. These constituents can inhibit crystallization, foul membranes, and co-precipitate, thereby affecting process performance. Therefore, validation with real wastewater is a necessary next step to assess practical feasibility of the integrated technology. Experimental campaigns with real wastewater should be planned to determine the effect of competing ions, suspended solids and organic matter on recovery efficiency and product quality (Buyukkamaci et al., 2023). These tests will provide information on potential pre-treatment steps prior to the integrated system.

In future work, artificial neural networks (ANNs) could be employed to capture more complex nonlinear behaviours once a larger dataset becomes available. Their demonstrated superior predictive accuracy in similar optimisation studies suggests strong potential for improving model robustness and extrapolation capability. Hybrid RSM–ANN approaches may further enhance optimisation efficiency and support deeper process understanding (Y. Liu et al., 2024).

When considering reactor scale-up, the long-term operation is necessary under dynamic conditions. The design of the upscaled reactor will require rethinking of the method of struvite collection and membrane mounting. Furthermore, eliminating the need for the feed heating or recycling heat at WWTPs could significantly reduce the cost of 1 kg $N_{removed}$ (Maktabifard et al., 2018).

Finally, concerning material and regulatory challenges, the current design employs PTFE-based hydrophobic membranes. While no formal regulations apply to WWTPs yet, there are growing concerns about using fluoropolymers in wastewater treatment due to their persistence and potential to release microplastics (Matavos-Aramyan, 2024). Therefore, exploring alternative GPM materials, such as polypropylene (PP), polyvinylidene fluoride (PVDF) and modified polymers, should be investigated for future use (Cao et al., 2024).

6. Conclusions

This study demonstrated the techno-economic feasibility of integrating struvite precipitation with NH_3-oriented GLMS for enhanced nutrient recovery from wastewater and confirmed the critical influence of pH, T and feed concentration on both processes. A key trade-off was identified between NH_3 volatilization, which drives GLMS, and NH_4^+ availability for struvite crystallization. Therefore, operating conditions at full scale should be selected to meet the specific objectives of each WWTP, balancing chemical and energy efficiency and recovered product purity. Nevertheless, regardless of the chosen scenario, the proposed one-reactor system represents a compact and effective solution facilitating compliance with the emerging EU wastewater regulations.

CRediT authorship contribution statement

Bogna Śniatała: Writing – original draft, Visualization, Methodology, Investigation, Data curation, Conceptualization. **Makinia Jacek:** Writing – review & editing, Supervision, Conceptualization. **Francesco Giannici:** Writing – original draft, Supervision, Resources, Methodology. **Giorgio Mannina:** Writing – review & editing, Supervision, Resources. **Dominika Sobotka:** Resources, Methodology, Funding acquisition. **Marta Ippolito:** Investigation.

Declaration of Competing Interest

The authors declare that they have no known competing financial interests or personal relationships that could have appeared to influence the work reported in this paper.

Acknowledgements

The research leading to these results has received funding from the Norway Grants 2014–2021 via the National Centre for Research and Development under the grant number NOR/SGS/INPORR/0074/2020–00.

Appendix A. Supporting information

Supplementary data associated with this article can be found in the online version at doi:10.1016/j.eti.2025.104686.

Data Availability

Data will be made available on request.

References

Achilleos, P., Roberts, K.R., Williams, I.D., 2022. Struvite precipitation within wastewater treatment: A problem or a circular economy opportunity? Heliyon 8, e09862. https://doi.org/10.1016/j.heliyon.2022.e09862.

Amaral, M.C., Magalhães, N.C., Moravia, W.G., Ferreira, C.D., 2016. Ammonia recovery from landfill leachate using hydrophobic membrane contactors. Water Sci. Technol. 74, 2177–2184. https://doi.org/10.2166/wst.2016.375.

Aryampa, S., Stuetz, R.M., Fisher, R.M., Luo, J., Wiedmann, T., 2025. Integrated recovery of nutrients during municipal wastewater treatment and biosolids management. J. Clean. Prod. 494, 144984. https://doi.org/10.1016/j.jclepro.2025.144984.

Bhuiyan, M.I.H., Mavinic, D.S., Koch, F.A., 2008. Thermal decomposition of struvite and its phase transition. Chemosphere 70, 1347–1356. https://doi.org/10.1016/j.chemosphere.2007.09.056.

Brandstätter, G., Fürsatz, K., Long, A., Hannl, T.K., Schubert, T., 2025. Exploring the potential of sewage sludge for gasification and resource recovery: A review. Environ. Technol. Innov. 40, 104346. https://doi.org/10.1016/j.eti.2025.104346.

Buyukkamaci, N., Karabacakogullari, S., Totur Pamik, D., 2023. Recovery of phosphorus from aqueous media as vivianite by crystallization. CLEAN Soil Air Water 51, 2300142. https://doi.org/10.1002/clen.202300142.

Cao, L., Wang, J., Xiang, S., Huang, Z., Ruan, R., Liu, Y., 2019. Nutrient removal from digested swine wastewater by combining ammonia stripping with struvite precipitation. Environ. Sci. Pollut. Res 26, 6725–6734. https://doi.org/10.1007/s11356-019-04153-x.

Cao, Z., Zhang, J., Deng, R., Wang, Z., Zhang, Z., Deng, B., Zhang, N., Zhang, Q., Wei, G., Liu, X., Xia, S., 2024. Enhanced ammonia recovery from wastewater by a transmembrane electro-chemisorption system directly connecting anode chamber and cathode chamber with gas permeable membrane. Chem. Eng. J. 485, 149554. https://doi.org/10.1016/j.cej.2024.149554.

Capdevielle, A., Sýkorová, E., Béline, F., Daumer, M.-L., 2016. Effects of organic matter on crystallization of struvite in biologically treated swine wastewater. Environ. Technol. 37, 880–892. https://doi.org/10.1080/09593330.2015.1088580.

Daneshgar, S., Cecconet, D., Capsoni, D., Capodaglio, A.G., 2022. Side-stream phosphorus recovery in activated sludge processes. Water 14, 1861. https://doi.org/10.3390/w14121861.

Emerson, K., Russo, R.C., Lund, R.E., Thurston, R.V., 1975. Aqueous ammonia equilibrium calculations: effect of pH and Temperature. J. Fish. Res. Bd. Can. 32, 2379–2383. https://doi.org/10.1139/f75-274.

EU 2024/, 3019. Directive (EU) 2024/3019 of the European Parliament and of the Council of 27 November 2024 concerning urban wastewater treatment.

Farghali, M., Chen, Z., Osman, A.I., Ali, I.M., Hassan, D., Ihara, I., Rooney, D.W., Yap, P.-S., 2024. Strategies for ammonia recovery from wastewater: a review. Environ. Chem. Lett. 22, 2699–2751. https://doi.org/10.1007/s10311-024-01768-6.

Gates-Rector, S., Blanton, T., 2019. The powder diffraction file: a quality materials characterization database. Powder Diffr. 34, 352–360. https://doi.org/10.1017/S0885715619000812.

Guan, Q., Li, Y., Zhong, Y., Liu, W., Zhang, J., Yu, X., Ou, R., Zeng, G., 2023. A review of struvite crystallization for nutrient source recovery from wastewater. J. Environ. Manag. 344, 118383. https://doi.org/10.1016/j.jenvman.2023.118383.

Günther, S., Grunert, M., Müller, S., 2018. Overview of recent advances in phosphorus recovery for fertilizer production. Eng. Life Sci. 18, 434–439. https://doi.org/10.1002/elsc.201700171.

Ha, T.-H., Mahasti, N.N.N., Ha, H.-Q., Liao, P.-L., Huang, Y.-H., Lu, M.-C., 2024. Recovery of nitrogen as struvite from swine wastewater: Comparison study of batch and continuous fluidized-bed crystallization process. Sep. Purif. Technol. 351, 128045. https://doi.org/10.1016/j.seppur.2024.128045.

Hao, X., Wang, C., Van Loosdrecht, M.C.M., Hu, Y., 2013. Looking Beyond Struvite for P-Recovery. Environ. Sci. Technol. 47, 4965–4966. https://doi.org/10.1021/es401140s.

Hollas, C.E., Bolsan, A.C., Venturin, B., Bonassa, G., Tápparo, D.C., Cândido, D., Antes, F.G., Vanotti, M.B., Szögi, A.A., Kunz, A., 2021. Second-generation phosphorus: recovery from wastes towards the sustainability of production chains. Sustainability 13, 5919. https://doi.org/10.3390/su13115919.

Krishnamoorthy, N., Dey, B., Unpaprom, Y., Ramaraj, R., Maniam, G.P., Govindan, N., Jayaraman, S., Arunachalam, T., Paramasivan, B., 2021. Engineering principles and process designs for phosphorus recovery as struvite: a comprehensive review. J. Environ. Chem. Eng. 9, 105579. https://doi.org/10.1016/j.jece.2021.105579.

Le, M.-V., Duy, T.H.T., Dang, B.-T., Luan, V.H., Huynh, N.-D.-T., Long, N.Q., Phuong, L.C.N., 2024. Phosphorus recovery from fertilizer industrial wastewaters using bittern: Influence of wastewater composition and pH on struvite formation. Bioresour. Technol. Rep. 25, 101752. https://doi.org/10.1016/j.biteb.2023.101752.
Le Corre, K.S., Valsami-Jones, E., Hobbs, P., Parsons, S.A., 2009. Phosphorus Recovery from Wastewater by Struvite Crystallization: A Review. Crit. Rev. Environ. Sci. Technol. 39, 433–477. https://doi.org/10.1080/10643380701640573.
Lecorre, K., Valsamijones, E., Hobbs, P., Jefferson, B., Parsons, S., 2007. Struvite crystallisation and recovery using a stainless steel structure as a seed material. Water Res. 41, 2449–2456. https://doi.org/10.1016/j.watres.2007.03.002.
Liu, Q., Sun, W., Zeng, Q., Zhang, H., Wu, C., Lichtfouse, E., Liu, H., 2024. Integrated processes for simultaneous nitrogen, phosphorus, and potassium recovery from urine: A review. J. Water Process Eng. 59, 104975. https://doi.org/10.1016/j.jwpe.2024.104975.
Liu, Y., Dar, B.N., Makroo, H.A., Aslam, R., Martí-Quijal, F.J., Castagnini, J.M., Amigo, J.M., Barba, F.J., 2024. Optimizing recovery of high-added-value compounds from complex food matrices using multivariate methods. Antioxidants 13, 1510. https://doi.org/10.3390/antiox13121510.
Luqmani, B., Brookes, A., Moore, A., Vale, P., Pidou, M., McAdam, E.J., 2024. Transitioning through the vapour-liquid equilibrium for low energy thermal stripping of ammonia from wastewater: Enabling transformation of NH3 into a zero-carbon fuel. Water Res. 248, 120856. https://doi.org/10.1016/j.watres.2023.120856.
Maktabifard, M., Zaborowska, E., Makinia, J., 2018. Achieving energy neutrality in wastewater treatment plants through energy savings and enhancing renewable energy production. Rev. Environ. Sci. Biotechnol. 17, 655–689. https://doi.org/10.1007/s11157-018-9478-x.
Matavos-Aramyan, S., 2024. Addressing the microplastic crisis: A multifaceted approach to removal and regulation. Environ. Adv. 17, 100579. https://doi.org/10.1016/j.envadv.2024.100579.
Meena, R.A.A., Yukesh Kannah, R., Sindhu, J., Ragavi, J., Kumar, G., Gunasekaran, M., Rajesh Banu, J., 2019. Trends and resource recovery in biological wastewater treatment system. Bioresour. Technol. Rep. 7, 100235. https://doi.org/10.1016/j.biteb.2019.100235.
Mehta, C.M., Khunjar, W.O., Nguyen, V., Tait, S., Batstone, D.J., 2015. Technologies to Recover Nutrients from Waste Streams: A Critical Review. Crit. Rev. Environ. Sci. Technol. 45, 385–427. https://doi.org/10.1080/10643389.2013.866621.
Meira, R.C.D.S., Paz, S.P.A.D., Corrêa, J.A.M., 2020. XRD-Rietveld analysis as a tool for monitoring struvite analog precipitation from wastewater: P, Mg, N and K recovery for fertilizer production. J. Mater. Res. Technol. 9, 15202–15213. https://doi.org/10.1016/j.jmrt.2020.10.082.
Melgaço, L., Robles-Aguilar, A., Meers, E., Mota, C., 2021. Phosphorus recovery from liquid digestate by chemical precipitation using low-cost ion sources. J. Chem. Tech. amp Biotech. 96, 2891–2900. https://doi.org/10.1002/jctb.6842.
Munasinghe-Arachchige, S.P., Abeysiriwardana-Arachchige, I.S.A., Delanka-Pedige, H.M.K., Cooke, P., Nirmalakhandan, N., 2021. Nitrogen-fertilizer recovery from urban sewage via gas permeable membrane: Process analysis, modeling, and intensification. Chem. Eng. J. 411, 128443. https://doi.org/10.1016/j.cej.2021.128443.
Ndeddy Aka, R.J., Agyekum-Oduro, E., Zhu, J., Wu, S., 2025. Integrating electrolytic struvite precipitation with ammonia scrubbing toward complete recovery of nitrogen and phosphorus from anaerobic digestate of poultry litter. Sep. Purif. Technol. 370, 133287. https://doi.org/10.1016/j.seppur.2025.133287.
Palakodeti, A., Azman, S., Rossi, B., Dewil, R., Appels, L., 2021. A critical review of ammonia recovery from anaerobic digestate of organic wastes via stripping. Renew. Sustain. Energy Rev. 143, 110903. https://doi.org/10.1016/j.rser.2021.110903.
Pradhan, S.K., Mikola, A., Heinonen-Tanski, H., Vahala, R., 2019. Recovery of nitrogen and phosphorus from human urine using membrane and precipitation process. J. Environ. Manag. 247, 596–602. https://doi.org/10.1016/j.jenvman.2019.06.046.
Renfrew, D., Vasilaki, V., Nika, E., Harris, E., Katsou, E., 2024. Tracing wastewater resources: Unravelling the circularity of waste using source, destination, and quality analysis. Water Res. 250, 120901. https://doi.org/10.1016/j.watres.2023.120901.
Rodrigues, M., Lund, R.J., Ter Heijne, A., Sleutels, T., Buisman, C.J.N., Kuntke, P., 2022. Application of ammonium fertilizers recovered by an Electrochemical System. Resour. Conserv. Recycl. 181, 106225. https://doi.org/10.1016/j.resconrec.2022.106225.
Sangeetha, V., Devasena, M., Nambi, I., Dwarakanathan, S., 2022. Crystallization of struvite family crystals from cow urine: analysis, characterization, and effects of crystallization method, retention time, rate of mixing, and competing ions. Biomass.. Convers. Biorefinery 14. https://doi.org/10.1007/s13399-022-02452-x.
Santos, A.F., Abreu, R.L., Alvarenga, P., Gando-Ferreira, L.M., Quina, M.J., 2024. An innovative two-step methodology for struvite recovery from wastewater with high purity and agronomic potential. J. Water Process Eng. 67, 106206. https://doi.org/10.1016/j.jwpe.2024.106206.
Serra-Toro, A., Vinardell, S., Astals, S., Madurga, S., Llorens, J., Mata-Álvarez, J., Mas, F., Dosta, J., 2022. Ammonia recovery from acidogenic fermentation effluents using a gas-permeable membrane contactor. Bioresour. Technol. 356, 127273. https://doi.org/10.1016/j.biortech.2022.127273.
Śniatała, B., Al-Hazmi, H.E., Sobotka, D., Zhai, J., Mąkinia, J., 2024. Advancing sustainable wastewater management: A comprehensive review of nutrient recovery products and their applications. Sci. Total Environ., 173446 https://doi.org/10.1016/j.scitotenv.2024.173446.
Śniatała, B., Sobotka, D., Szeląg, B., Mąkinia, J., 2025. Optimization of liquid-to-liquid membrane stripping for ammonia removal and recovery: The influence of key operational parameters on process performance. J. Environ. Chem. Eng. 13, 119309. https://doi.org/10.1016/j.jece.2025.119309.
Soto-Herranz, M., Sánchez-Báscones, M., Antolín-Rodríguez, J.M., Vanotti, M.B., Martín-Ramos, P., 2021. Effect of acid flow rate, membrane surface area, and capture solution on the effectiveness of suspended gpm systems to recover ammonia. Membranes 11, 538. https://doi.org/10.3390/membranes11070538.
Sun, L., Yang, Y., Yuan, W., Wu, X., Cui, Z., Wang, H., Deng, H., Zhu, X., Li, R., 2023. Struvite purity prediction by response surface methodology and chemical equilibrium modeling combination. Environ. Technol. Innov. 29, 103016. https://doi.org/10.1016/j.eti.2023.103016.
Tansel, B., Lunn, G., Monje, O., 2018. Struvite formation and decomposition characteristics for ammonia and phosphorus recovery: A review of magnesium-ammonia-phosphate interactions. Chemosphere 194, 504–514. https://doi.org/10.1016/j.chemosphere.2017.12.004.
Tian, X., Gao, Z., Feng, H., Zhang, Z., Li, J., Wang, A., 2019. Efficient nutrient recovery/removal from real source-separated urine by coupling vacuum thermal stripping with activated sludge processes. J. Clean. Prod. 220, 965–973. https://doi.org/10.1016/j.jclepro.2019.02.181.
Toby, B.H., Von Dreele, R.B., 2013. *GSAS-II*: the genesis of a modern open-source all purpose crystallography software package. J. Appl. Crystallogr 46, 544–549. https://doi.org/10.1107/S0021889813003531.
Tran, Q., Oak, J.J., Kim, J., Jin, X., 2025. Enhancing nutrient water recovery: An integrated electrodialysis – Forward osmosis approach for reduced energy consumption and membrane fouling. Sep. Purif. Technol. 357, 130164. https://doi.org/10.1016/j.seppur.2024.130164.
Vaneeckhaute, C., Lebuf, V., Michels, E., Belia, E., Vanrolleghem, P.A., Tack, F.M.G., Meers, E., 2017. Nutrient Recovery from Digestate: Systematic Technology Review and Product Classification. Waste Biomass.. Valor 8, 21–40. https://doi.org/10.1007/s12649-016-9642-x.
Wan, Y., Li, R., Wang, X., Liao, C., 2023. Recovery of reactive nitrogen from wastewater using bioelectrochemical systems. Sep. Purif. Technol. 327, 125002. https://doi.org/10.1016/j.seppur.2023.125002.
Wen, L., Peng, L.E., Li, X.-Y., 2021. Contactless membrane distillation for effective ammonia recovery from waste sludge: A new configuration and mass transfer mechanism. J. Membr. Sci. 638. https://doi.org/10.1016/j.memsci.2021.119733.
Wu, H., Vaneeckhaute, C., 2022. Nutrient recovery from wastewater: a review on the integrated Physicochemical technologies of ammonia stripping, adsorption and struvite precipitation. Chem. Eng. J. 433, 133664. https://doi.org/10.1016/j.cej.2021.133664.
Yan, Y., Kallikazarou, N.I., Nisiforou, O., Shang, Q., Fu, D., Antoniou, M.G., Fotidis, I.A., 2025. Phosphorus recovery through struvite crystallization from real wastewater: Bridging gaps from lab to market. Bioresour. Technol. 427, 132408. https://doi.org/10.1016/j.biortech.2025.132408.
Yang, K., Qin, M., 2024. Understanding Ammonia and Water Transport in Direct Contact Membrane Distillation toward Selective Ammonia Recovery. ACS EST Eng. 4, 1321–1330. https://doi.org/10.1021/acsestengg.3c00623.
Yu, R., Ren, H., Wang, Y., Ding, L., Geng, J., Xu, K., Zhang, Y., 2013. A kinetic study of struvite precipitation recycling technology with NaOH/Mg(OH)2 addition. Bioresour. Technol. 143, 519–524. https://doi.org/10.1016/j.biortech.2013.06.042.
Zaffar, A., Jayaraman, S., Sutar, P.P., Balasubramanian, P., 2024. Comparative evaluation of drying methods for struvite produced from electrocoagulated source-separated urine: Implications for quality, energy and cost-effectiveness. J. Environ. Manag. 356, 120665. https://doi.org/10.1016/j.jenvman.2024.120665.
Zhou, T., Xu, N., Chen, G., Zhang, M., Ji, T., Feng, X., Wang, C., 2024. Magnesium source with function of slowly releasing Mg and pH control for impurity-resistance synthesis ultra-large struvite from wastewater. Sci. Total Environ. 924, 171636. https://doi.org/10.1016/j.scitotenv.2024.171636.
Zhu, Y., Chang, H., Yan, Z., Liu, C., Liang, Y., Qu, F., Liang, H., Vidic, R.D., 2024. Review of ammonia recovery and removal from wastewater using hydrophobic membrane distillation and membrane contactor. Sep. Purif. Technol. 328, 125094. https://doi.org/10.1016/j.seppur.2023.125094.